Invited Paper

Sub-nanometer Calibration of CD-SEM Line Width by Using STEM

Kiyoshi Takamasu*[a], Kazuki Kuwabara[a], Satoru Takahashi[a],
Takeshi Mizuno[b], Hiroki Kawada[b]
[a]The University of Tokyo, Hongo 7-3-1, Bunkyo-ku, Tokyo, JAPAN 113-8656;
[b]Hitachi High-Technologies Corp., Ichige 882, Hitachinaka-shi, Ibaraki-ken, JAPAN 312-8504

ABSTRACT

The novel calibration method of sub-nanometer accuracy for the line width measurement using STEM images is proposed to calibrate CD-SEM line width measurements. In accordance with the proposed method, the traceability and reference metrology of line width standards are established using Si lattice structures. First, we define the edge of a line as the end of Si lattice structure as the interface between Si lattice and oxide film. Second, an image magnification and inclination angles are calculated using 2D Fourier analysis of a STEM image. Third, the edge positions of the line are detected after the novel noise reduction method using averaging by Si lattice patterns. Then, the uncertainty of the line width measurement is evaluated with the uncertainty contributors of pixel size, edge detections and repeatability. Using the proposed method, the expanded uncertainty less than 0.5 nm for the line width of 45 nm is established.

Keywords: line width standard, traceability, uncertainty, Si lattice, STEM, CD-SEM, reference metrology, calibration

1. INTRODUCTION

The line width measurement in semiconductor industry is mainly carried out by CD-SEM (Critical Dimension Scanning Electron Microscope). The sub-nanometer repeatability of the line width measurement can be obtained using CD-SEM[1-3]. However, absolute accuracy of the line width measurement is not evaluated, and traceability is not established in the measurement[4-6]. The absolute accuracy of the line width is recently in great demand for physical simulations such as spectrometry and performance evaluation of transistors. Therefore, we started to develop the novel method of line width measurements with high absolute accuracy.

In this article, the novel method of sub-nanometer accuracy for the line width measurement using STEM (Scanning Transmission Electron Microscope) images is proposed to calibrate CD-SEM and CD-AFM line width measurements. In accordance with the proposed method, the traceability and reference metrology of line width standards are established using Si lattice patterns and the uncertainty of the line width measurement is evaluated. The targets of the study as follows:

- The definition of the line width is clearly defined.
- Novel data processing procedure for STEM image is determined.
- Novel edge detection method is proposed.
- Traceability is established by the uncertainty estimation on the proposed method.

The comparisons between methods with sectional images by STEM or sectional SEM and methods with horizontal images by CD-SEM or CD-AFM are shown in Figure 1. Using the sectional images, edge positions of a line are clearly observed by STEM and sectional SEM. Furthermore, because the Si lattice structure is observed in STEM images, the image magnification is precisely estimated. From these reasons, we select to use STEM in the methods of investigation for the line width[7-10] shown in Table 1.

Then, the uncertainty of the line width measurement is evaluated with the uncertainty contributors of pixel size, edge detections and repeatability. Using the proposed method, the expanded uncertainty less than 0.5 nm for the line width of 45 nm is established.

*takamasu@pe.t.u-tokyo.ac.jp; phone 81 3 5841-6450; fax 81 3 5841-8554; www.nanolab.t.u-tokyo.ac.jp

Metrology, Inspection, and Process Control for Microlithography XXIV, edited by Christopher J. Raymond,
Proc. of SPIE Vol. 7638, 76381K · © 2010 SPIE · CCC code: 0277-786X/10/$18 · doi: 10.1117/12.846436

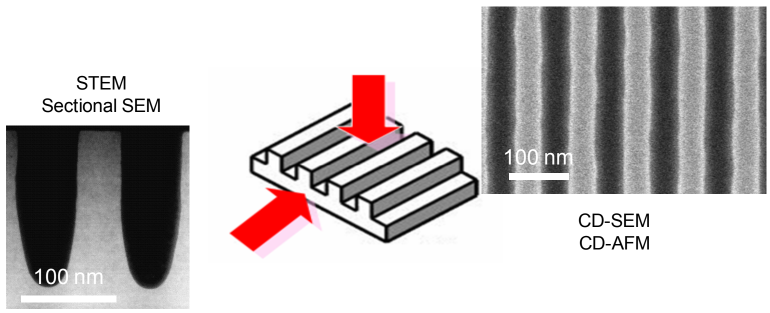

Figure 1. Comparisons between a sectional image by STEM or sectional SEM and a horizontal image by CD-SEM or CD-AFM

Table 1. Comparisons of investigation methods for the line width measurements.

items	STEM	Sectional SEM	CD-SEM	CD-AFM
direction	sectional	sectional	horizontal	horizontal
accuracy	best	good	good	good
magnification calibration	Si lattice constant	pitch standard	pitch standard	pitch standard
offset evaluation	Si lattice	simulation	simulation	line width standard
measuring range	small	small	small	large
measuring time	long	long	short	short
destructive	yes	yes	no	no

2. STEM IMAGES AND DATA PROCESSING

2.1 Sample for STEM and Si lattice image

Three types STEM images can be obtained as a bright field phase contrast image by transmission electron, a bright field scattering-absorption contrast image by transmission electron, and a dark field image by scattered electron shown in Figure 2. The Si lattice structures are clearly observed by the bright field phase contract image. Therefore, this type of image is used to define the proposed method in this article. Figure 3 (a) illustrates a thin specimen thickness of 100 nm. The specimen is a standard of line width of Si wafer, and it is sliced on Si 110 surface by FIB (Focused Ion Beam) micro sampling system[11]. Then the STEM images of the specimen are obtained by STEM[12] (HD-2700) with accelerating voltage of 200 kV and magnification of 70,000 to 3,000,000. The terms such as a line width, a pitch, a height and an edge are defined in Figures 3 (b) and (c).

The STEM images under deferent magnifications are shown in Figure 4. The high magnification STEM image shows Si lattice structures clearly (Figures 4 (c) and (d)). The lattice parameter[13,14] of Si is defined as 0.543102064 nm with very small uncertainty of 0.000000014 nm. We can use the lattice constant of Si as the scale to calibrate the magnification of STEM images.

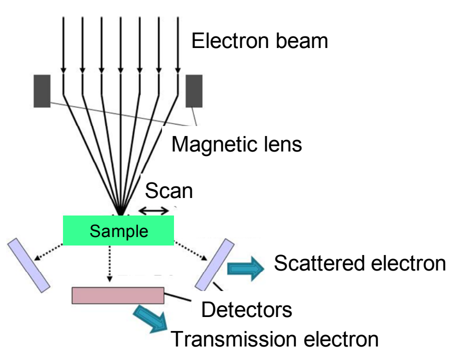

Figure 2. Construction of STEM with two types of detectors for scattered electron and transmission electron.

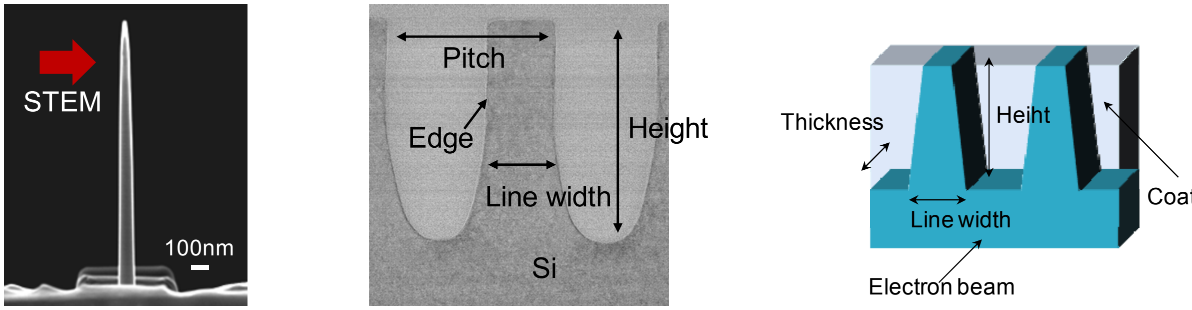

(a) (b) (c)

Figure 3. Sample for STEM and Si lattice image; (a) thin specimen of 100 nm thickness by FIB (Focused Ion Beam) micro sampling system, (b) STEM image of standard line width on the Si wafer on Si 110 surface, and (c) the model of line width.

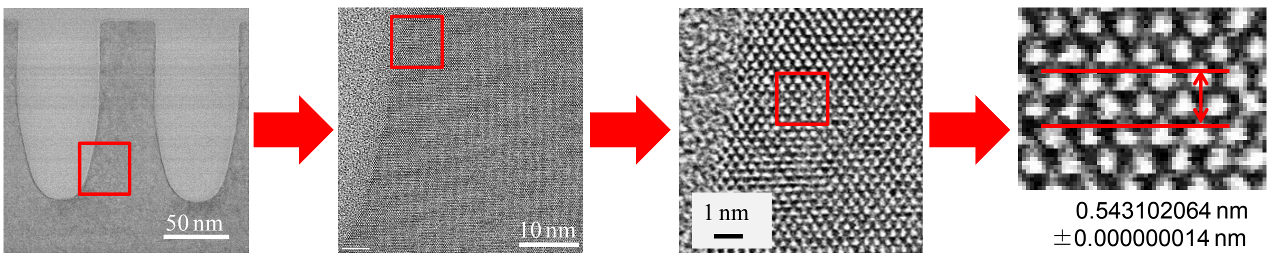

(a) (b) (c) (d)

Figure 4. Si lattice structures are observed by a STEM bright field phase contrast image under the deferent image magnifications. The lattice parameter of Si is defined as 0.543102064 nm with uncertainty of 0.000000014 nm.

2.2 Image parameters of STEM image by 2D Fourier analysis

Si lattice structure is observed clearly on the high magnification STEM images. The image parameters as a pixel size and inclination angles of the image are calculated using 2D Fourier analysis. Figure 5 (a) is an example of STEM image with accelerating voltage of 200 kV and magnification of 3,000,000. The inside of Si lattice (red frame of 700 × 700 pixels) is extracted and transformed to a frequency domain image (Figure 5 (b)) with zero padding method[15,16]. The positions of peaks of the frequency domain image shown in Table 2 are compared with the Si lattice pattern (Figure 5 (c)), then, an image pixel size and inclination angles of the image are calculated. For the image, the pixel size is calculated as 0.04124 nm/pixel and the inclination angles are calculated as 0.978 arc-degree on X direction and 0.240 arc-degree on Y direction. The inclination angles are mainly caused by drifts during STEM scanning.

The variation of pixel size is calculated in four frames at deferent positions of the STEM image. From these calculations, we estimated the standard deviation of magnification is less than 0.149 %.

Table 2. Positions of four main peaks (Figure 5 (b)) on the frequency domain image by 2D Fourier analysis of the STEM image (Figure 5 (a)) with zero padding method.

peaks	X position (pixel)	Y position (pixel)
Origin	2501	2501
Peak 1	2488	1739
Peak 2	3031	2118
Peak 3	3575	2496
Peak 4	3045	2880

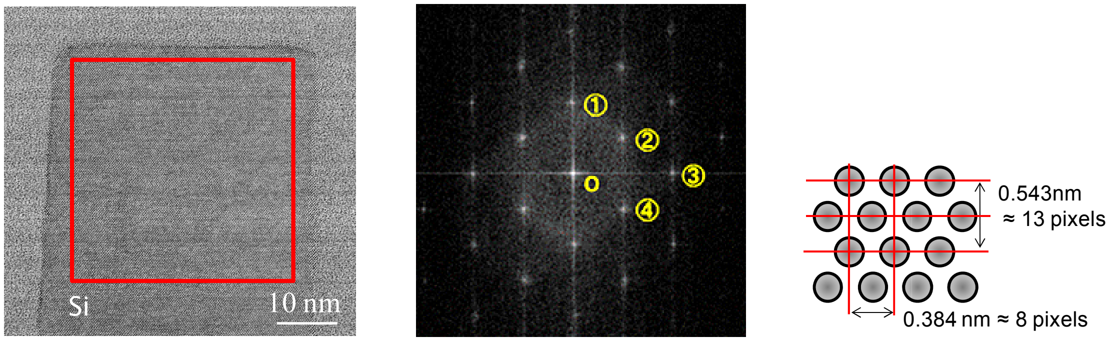

(a) (b) (c)

Figure 5. 2D Fourier analysis of STEM image; (a) inside of red frame (700 × 700 pixels) is extracted, (b) transformed to a frequency domain image with zero padding and four main peaks, and (c) the model of Si lattice structure.

2.3 Image intensity graph

Figure 6 (a) shows an example of STEM image, and the horizontal axis is defined as X axis and the vertical axis is defined as Y axis. Then Figure 6 (b) displays an example of an intensity graph on the yellow line of Figure 7 (a). For the intensity graph, the horizontal axis is defined as X axis and the vertical axis is defined as intensity of each pixel of X position in the STEM image. Figure 6 (c) shows the enlarged view of left edge of the intensity graph (Figure 7 (b)).

When the noise of the STEM image is low, the edge of line may be detected by the intensity graph with a certain threshold level. However, the edge position detected by the threshold level is influenced by the image conditions and the threshold level of edge definitions.

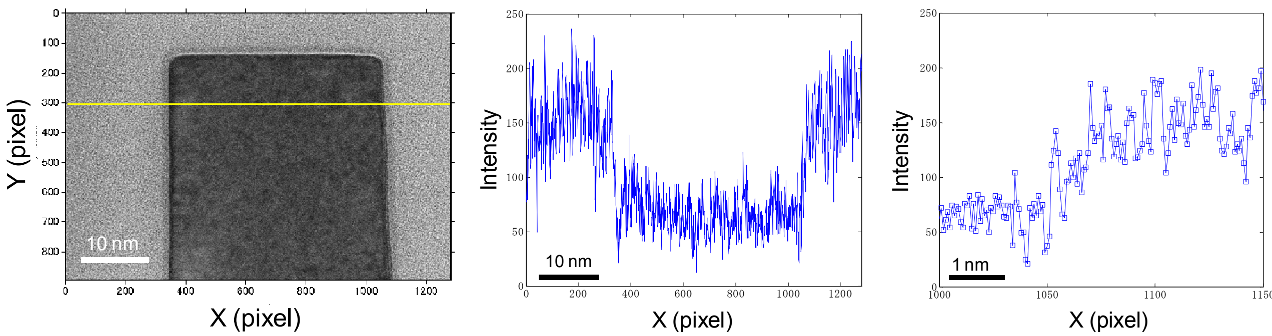

(a) (b) (c)

Figure 6. STEM image and an intensity graph; (a) example of STEM image, (b) example of an intensity graph on the yellow line, (c) enlarged view of the left edge.

2.4 Image rotation

Before detection of edge positions of the line, the image is rotated by the inclination angles detected on section 2.2. Figure 7 (a) shows a STEM image and Si lattice line of the image as the yellow lines. Figure 7 (b) shows the horizontal image and the intensity graph on the yellow line of the image, and the Si lattice pattern can be observed as a zigzag line in the intensity graph. However, the intensity of zigzag line at the far left is week because of inclination of the image. Then, Figure 7 (c) shows a STEM image after the rotation by the incline angles detected by 2D Fourier analysis. Figure 7 (d) shows the zigzag line image in the intensity graph clearly on the left part of the graph.

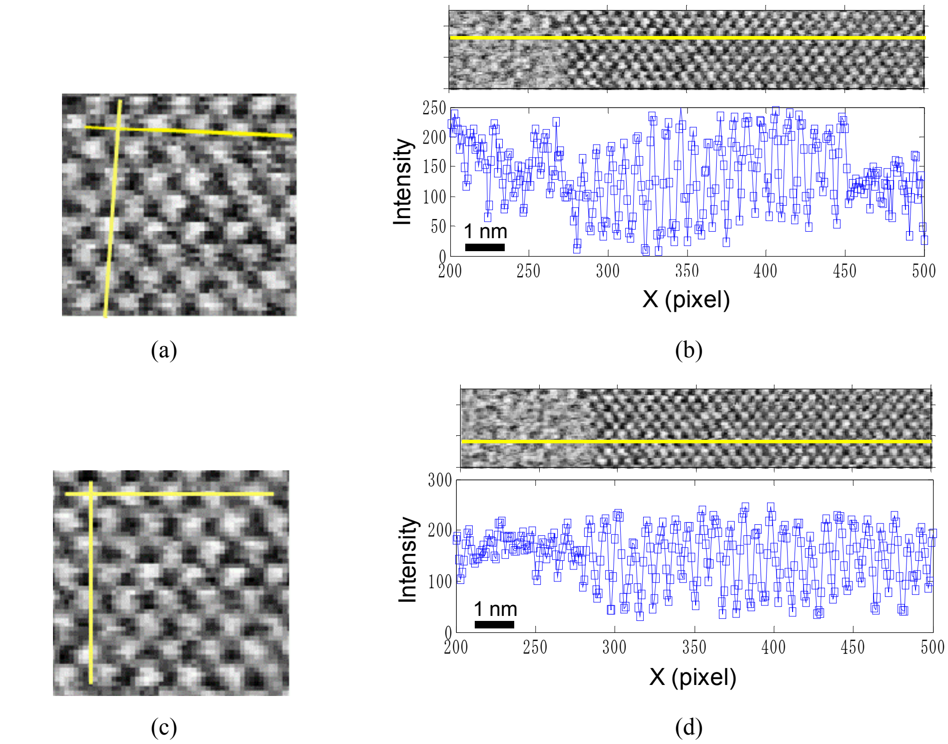

Figure 7. Image rotation of the Si lattice structure in the STEM image; (a) STEM image before rotation, (b) horizontal image and image intensity graph before rotation, (c) STEM image after rotation, and (d) horizontal image and image intensity graph after rotation.

3. EDGE DETECTION AND LINE WIDTH CALCULATION

3.1 Definition of edge

Figure 8 (a) shows an example of a bright field phase contrast STEM image. In this image, Si lattice structure, oxide film and coating can be observed. The thickness of the oxide film varies under circumstance conditions such as atmosphere gas density, temperature, gas pressure, and exposure time for gas. Therefore, we define the edge as the end of Si lattice structure. Figure 8 (b) shows the intensity graph on the yellow line of Figure 8 (a), and it indicates that the interface between the Si lattice structure and the oxide film as a red circle. The study for thickness of the oxide film will be precisely analyzed for our future works.

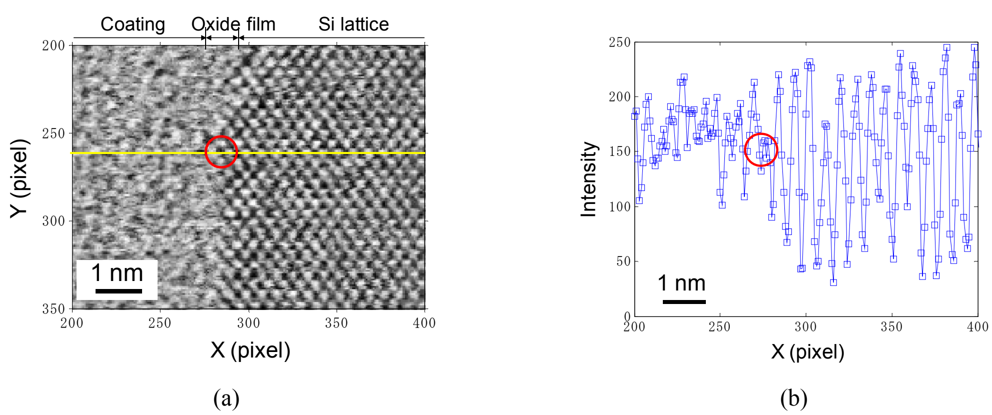

Figure 8. Definition of the edge (red circle) as the end of Si lattice structure between Si lattice and oxide film; (a) example of a bright field phase contrast STEM image, and (b) intensity graph on the yellow line.

3.2 Averaging by Si lattice pattern

Noise of STEM images is influenced by magnification of image, scanning speed of STEM, and conditions of the specimen. Assuming that the noise is random, simple averaging method is normally applied. However, the simple averaging method reduces not only noise but also Si lattice pattern. Therefore, the novel averaging method is proposed using Si lattice pattern. The Si lattice pattern on Si 110 surface is well known as Figure 9 (a). The size of X pitch of the lattice (0.384 nm) is approximately 9 pixels and the size of Y pitch (0.5432 nm) is approximately 13 pixels in the image.

The two deferent size stencil patterns for the averaging method using the Si lattice pattern are shown on Figures 9 (b) and (c). The small pattern (Figure 9 (b)) consists of 140 pixels (10 × 14 pixels), and the averaging is done only on 20 pixels as the red pixels. The horizontal and vertical intervals of the stencil agree with the positions of 5 lattices, therefore, the random noise is reduced and the lattice structures are emphasized. The large pattern (Figure 9 (c)) is 18 × 26 pixels, and it agrees with the positions of 13 lattices. Then, the stencil moves on the image two dimensionally shown in Figure 10. The proposed averaging method emphasizes the Si lattice positions and reduces the random noise out of Si lattice positions.

An example of the averaging method is shown in Figure 11. Figure 11 (a) is a part of the Si lattice image and the intensity graph on the yellow line before averaging, Figures 11 (b) and (c) are the averaging Si lattice images and the intensity graphs of them using the small and large stencil patterns, respectively. The random noise is reduced and the Si lattice positions are clearly founded in the images.

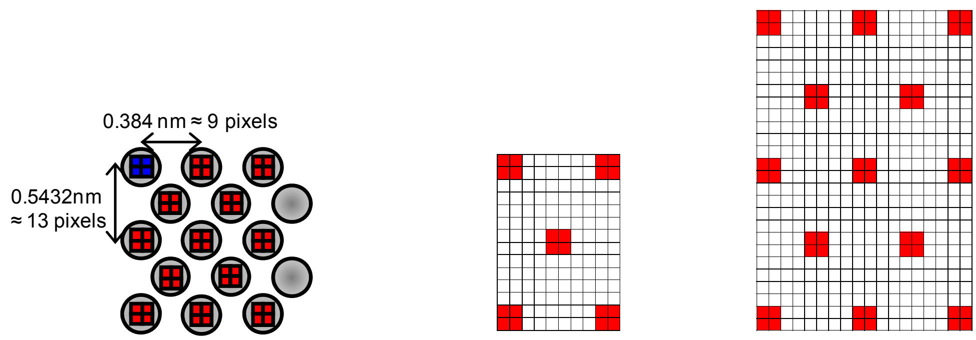

(a) (b) (c)

Figure 9. Stencil for averaging method; (a) pattern of Si lattice structure on Si 110 surface, (b) small stencil pattern (10 × 14 pixels) on 5 lattices, and (c) large stencil pattern (18 × 26) on 13 lattices.

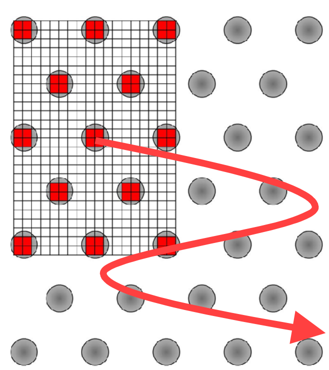

Figure 10. Stencil moves on the STEM image two dimensionally, and then random noise is reduced and Si lattice patterns are emphasized.

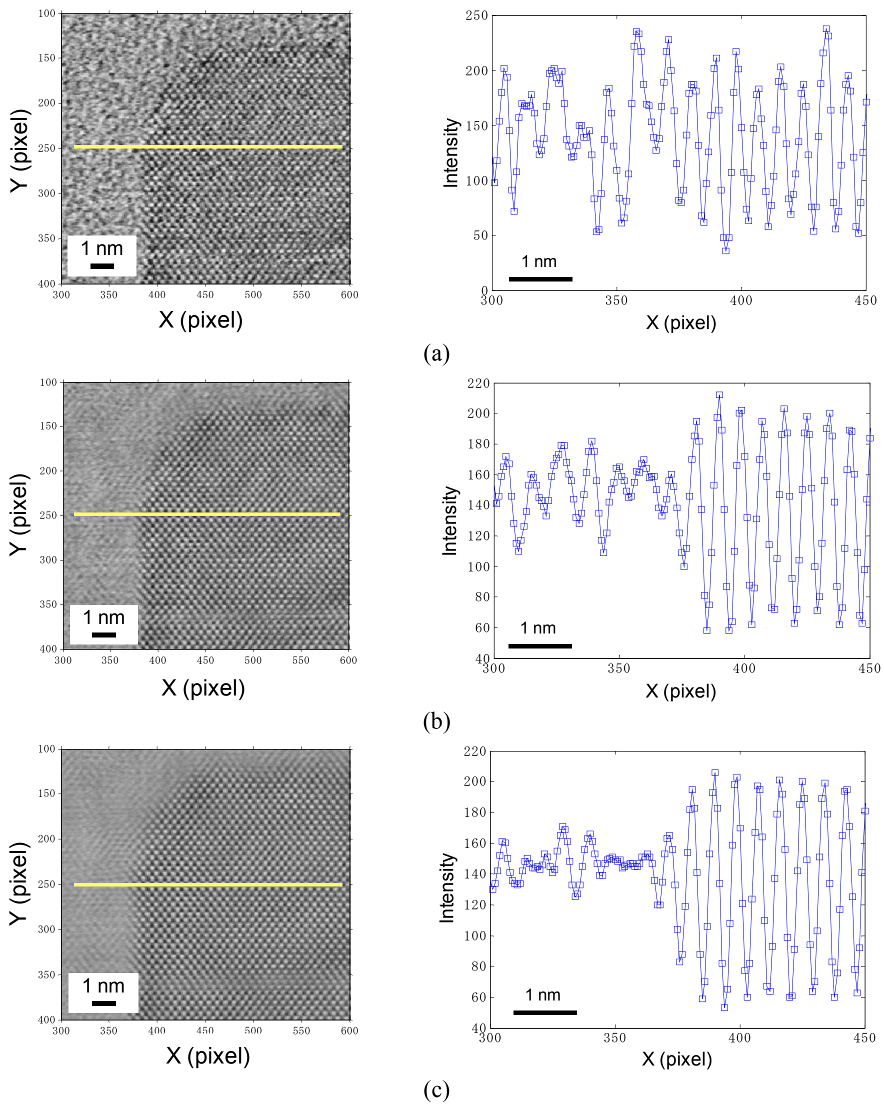

Figure 11. Examples of the proposed averaging method using Si lattice pattern: (a) Si lattice image and the intensity graph before averaging, (b) averaging Si lattice image and the intensity graph using the small stencil pattern, and (c) averaging Si lattice image and the intensity graph using the large stencil pattern.

3.3 Edge detection using local standard deviation of the Si lattice image

After averaging the image, the method to detect the edge is developed under the consideration of the Si lattice structure. The method to detect the edge using the intensity of STEM image is influenced by the image conditions and threshold level of the definition of the edge. Therefore, we define the edge is the end of Si lattice pattern, and then the end of the Si lattice pattern is detected. Figures 12 (a) and (b) illustrate the frames for the calculation method of local standard deviation. We use the small rectangle frame (8×12 pixels) and the large rectangle frame (16×24 pixels) to calculate the local standard deviation of the image. If the size of the specified area to calculate the local standard deviation is used as the size of Si lattice, the effect of Si lattice on the local standard deviation is reduced.

The local standard deviation inside of the rectangle frame is calculated, and the frame moves two dimensionally (Figure 12 (c)), and the local standard deviation image (Figure 12 (d)) is obtained. Figure 12 (e) shows the local standard deviation graph on the red line of the local standard deviation image. The value of local standard deviation clearly indicates the end of Si lattice structure, and then the position of 50 % of the local standard deviation value is defined as the edge of Si lattice structure. The average deviation of the threshold level is 0.15 pixel, and then the standard uncertainty of line width by the threshold level is evaluated at 0.007 nm.

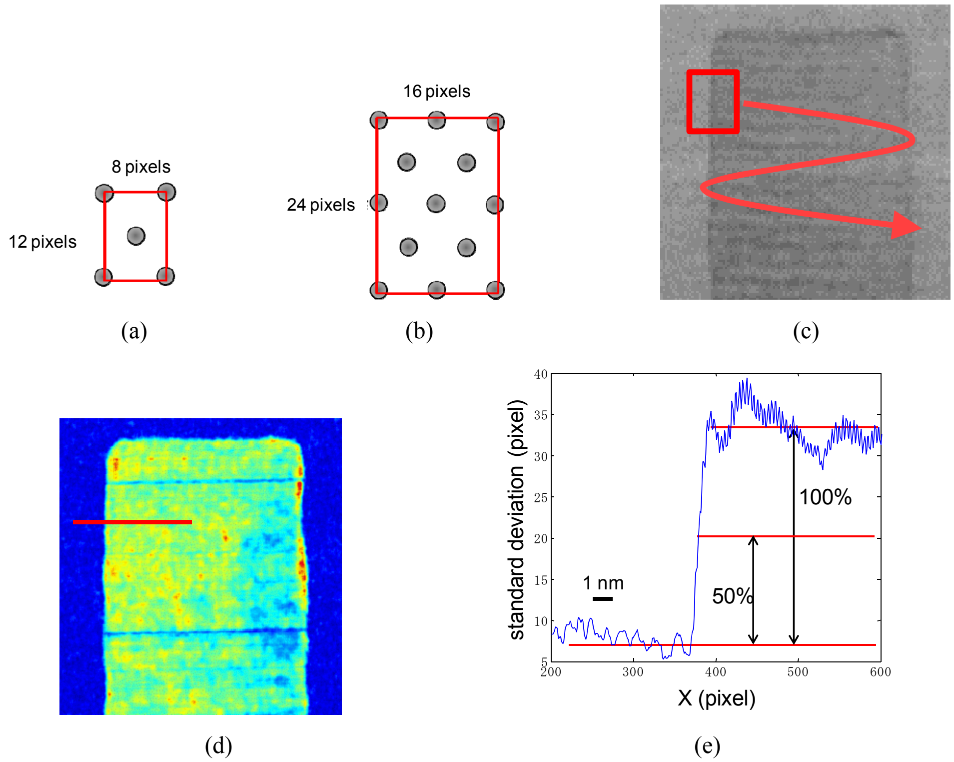

Figure 12. Calculation method of the local standard deviation of the specified area (red rectangle frame); (a) small rectangle frame (8 × 12 pixels), (b) large rectangle frame (16 × 24 pixels), (c) rectangle frame moves two dimensionally on the STEM image, (d) local standard deviation image, and (e) local standard deviation graph on the red line, the 50 % point is defined as the edge of Si lattice structure.

3.4 Example of edge detection

We defined the procedure to detect the edge of Si lattice structure on sections 3.2 and 3.3. Figure 13 demonstrates an example of the procedure of the proposed method for the STEM image with accelerating voltage of 200 kV and magnification of 2,800,000 as the follows:

- Original STEM image (Figure 13 (a)),
- Rotated STEM image (Figure 13 (b)),
- Averaging STEM image (Figure 13 (c)),
- Local standard deviation image (Figure 13 (d)),
- Detected edges on the averaging STEM image (Figure 13 (e)), and.
- Detected edges on the rotated STEM image (Figure 13 (f))).

The experimental conditions for Figure 13 are described in Table 3. Figure 14 (a) shows the detail of left and right edge detections on the averaging image (Figure 13 (e)) and Figure 14 (b) shows that on the rotated image (Figure 13 (f)). In Figure 14, the red line is detected edge using the small frame of 8 × 12 pixels for the local standard deviation image and the yellow line is that using the large frame of 16 × 24 pixels.

Table 3. Experimental conditions for the edge detection in Figure 13.

items	descriptions
STEM image	magnification of 2,800,000 with accelerating voltage of 200 kV
image size	1600 × 3500 pixels from 4096 × 4096 pixels
pixel size	0.04428 nm/pixel
incline angles	1.25 arc-degree on X direction, 2.24 arc-degree on Y direction
averaging stencil size	18 × 26 pixels
standard deviation frame size	8 × 12 or 16 × 24 pixels

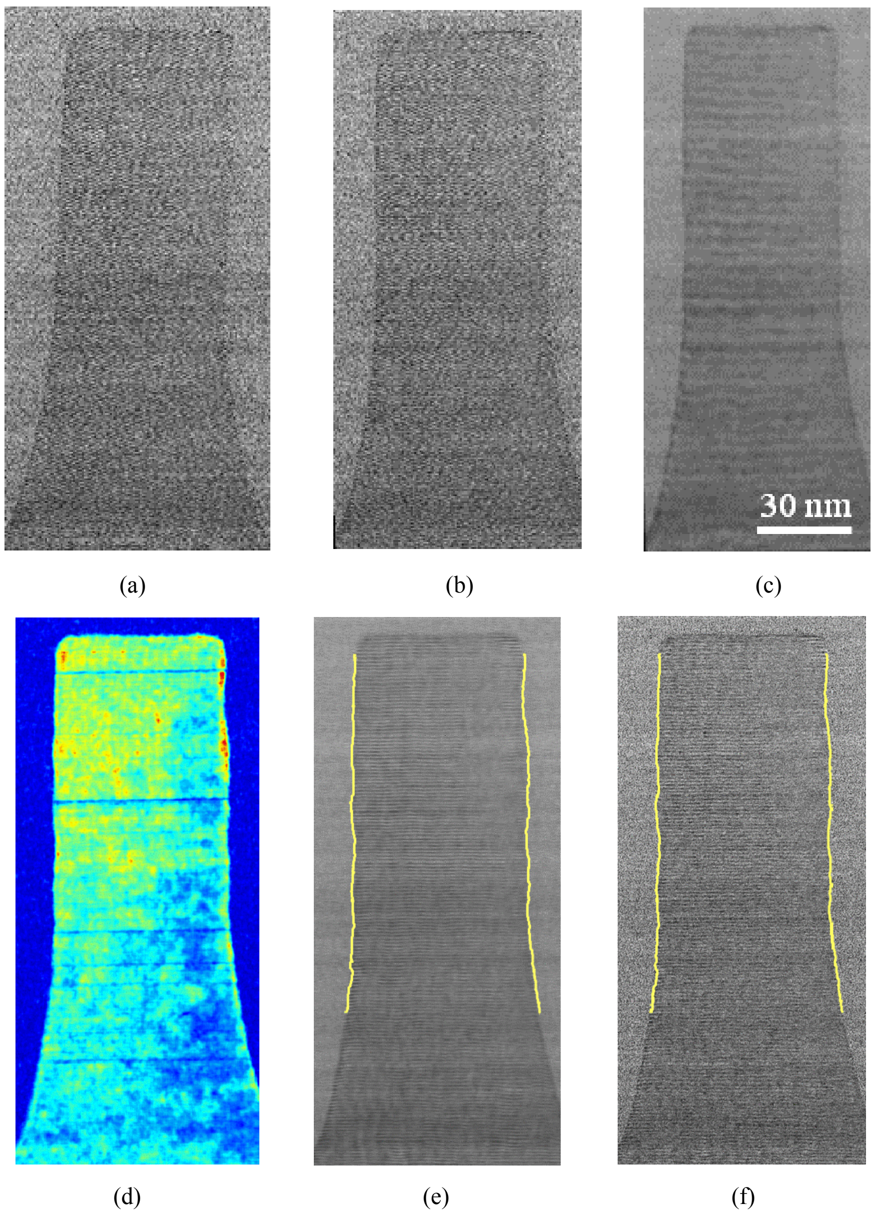

Figure 13. Example of the edge detection for the STEM image with accelerating voltage of 200 kV and magnification of 2,800,000; (a) original STEM image, (b) rotated STEM image, (c) averaging STEM image, (d) local standard deviation image, (e) detected edges on the averaging STEM image, and (f) detected edges on the rotated STEM image.

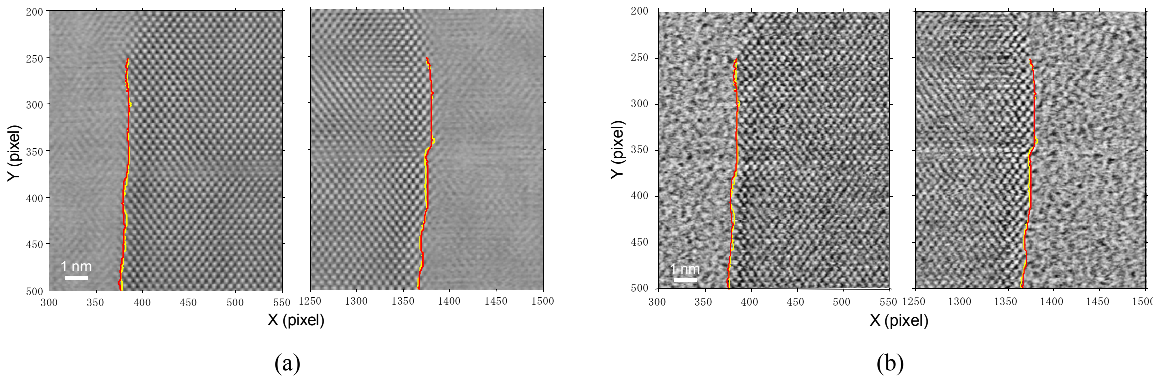

Figure 14. Details of the edge detections; (a) on the averaging image (Figure 13 (e)), and (b) on the rotated image (Figure 13 (f)). The yellow lines are the detected edges using 8 × 12 pixels frame for the local standard deviation image and the red lines are those using 16 × 24 pixels frame.

3.5 Line width calculation

The line width is calculated by the positions of the right edge and the left edge, and the pixel size of the STEM image shown in Figure 15 (a). Equation (1) shows the calculation of line width w (nm), where e_r is the right edge position (pixel), e_l is the left edge position (pixel), u is line width pixel size (pixel) and p is pixel size (nm/pixel).

$$w = (e_r - e_l) \cdot p = u \cdot p. \tag{1}$$

The line widths are calculated at Y axis positions indicated on Figure 15 (b). The line width is evaluated on 0.9 nm area at each Y position. Table 4 describes the averaged line widths at these positions and the standard deviations. The standard deviation of the edge positions is around 0.063 nm. The average line width is the average of 20 lines on 0.9 nm area, and then the standard uncertainty by Y positions is evaluated 0.014 nm as 0.063 nm divided by square root of 20.

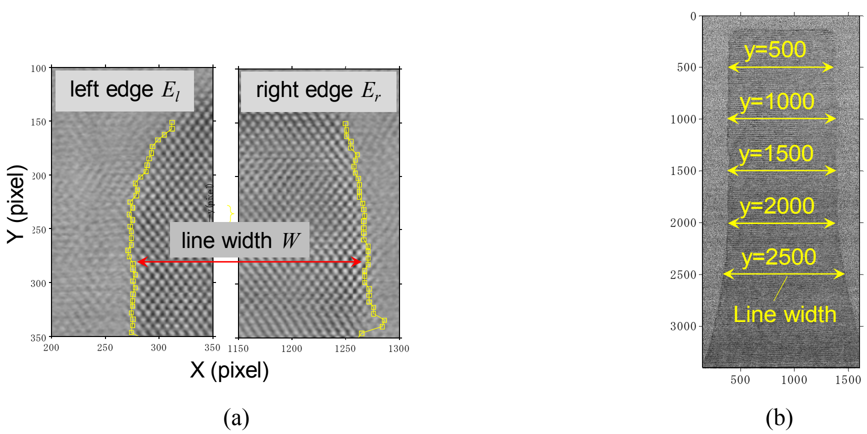

Figure 15. Line width calculation; (a) positions of left edge and right edge, and (b) Y positions for the evaluations.

Table 4. Average line widths and deviations on 0.9 nm area at the specified Y positions.

Y position (pixel)	standard deviation; frame size 8 × 12		standard deviation; frame size 16 × 24	
	average line width (nm)	deviation (nm)	average line width (nm)	deviation (nm)
500	43.85	0.048	43.95	0.038
1000	45.28	0.074	45.38	0.077
1500	44.86	0.058	44.95	0.039
2000	46.10	0.034	46.20	0.037
2500	50.13	0.101	50.23	0.058

3.6 Uncertainty evaluation for the line width calculation

From partial differential of Equation (1), Equation (2) shows the uncertainty of line width s_w propagated by the uncertainty of pixel size s_p and that of line width detection s_u. From the relative uncertainty of pixel size s_p/p is evaluated at 0.149 % in Section 2.2, the standard uncertainty by pixel size us_p is 0.067 nm when the line with w is 45 nm.

The uncertainty of line width detection ps_u is evaluated from the following uncertainty contributors (unit is nm):

- position on Y axis ps_{u1},
- threshold level of edge detection ps_{u2}, and
- repeatability ps_{u3}.

$$
\begin{aligned}
s_w &= \sqrt{\left(\frac{\partial w}{\partial u} s_u\right)^2 + \left(\frac{\partial w}{\partial p} s_p\right)^2} = \sqrt{(ps_u)^2 + (us_p)^2}, \\
ps_u &= \sqrt{(ps_{u1})^2 + (ps_{u2})^2 + (ps_{u3})^2}, \\
us_p &= \frac{s_p}{p} w.
\end{aligned}
\tag{2}
$$

The uncertainty contributor by position on Y axis (ps_{u1}) is evaluated at 0.014 nm in Section 3.5, and that by threshold level (ps_{u2}) is evaluated at 0.007 nm in Section 3.3. The uncertainty by repeatability (ps_{u3}) is evaluated by three iterations at 0.107 nm. From these results, we estimated that the standard uncertainty of line width detection (ps_u) is 0.108 nm. Therefore, the standard uncertainty of line width s_w is calculated from Equation (2) as 0.127 nm and the expanded uncertainty of 3σ is 0.381 nm (Table 5). For the further evaluation and comparisons with CD-SEM and CD-AFM, we will estimate the other contributors and the thickness of oxide film under different conditions.

Table 5. Uncertainty evaluation for the line width calculation (line width is 45 nm).

contributors	pixel size us_p	line width detection ps_u		
		position on Y axis ps_{u1}	threshold level ps_{u2}	repeatability ps_{u3}
evaluation	0.149 %	0.014 nm	0.15 pixel	0.239 %
standard uncertainty (measured)	0.067 nm	0.014 nm	0.007 nm	0.107 nm
		0.108 nm		
combined standard uncertainty σ	0.127 nm			
expand uncertainty 3σ	0.381 nm			

4. CONCLUSIONS AND FUTURE WORKS

The novel method of sub-nanometer accuracy for the line width measurement using STEM images is proposed to calibrate of CD-SEM line width measurement. In the proposed method, the traceability and reference metrology of line width standards are established using Si lattice structures. Using STEM images, the line width is calculated the following procedure:

- We define the edge of the line as the interface between the Si lattice structure and the oxide film.
- The image magnification (pixel size) and inclination angles of the STEM image are calculated by the peeks of the frequency domain image using 2D Fourier analysis.
- The image is rotated by the inclination angles.
- The proposed averaging method using the stencil emphasizes the Si lattice positions and reduces the random noise out of Si lattice positions.

- The edge position on the each Si lattice line is defined at the 50 % intensity of the local standard deviation of the STEM image.
- Line widths are calculated using the pixel size and the edge positions.
- Uncertainty of the line width measurement is evaluated.

The proposed method was applied to an example of Si line specimen, and the line width is calculated with the expand uncertainty (3σ) of 0.381 nm. In future works, we will compare the line width by STEM images using the proposed method and the results by CD-SEM images and CD-AFM images on the same line position. Then the detailed estimation of the uncertainty of the proposed method is calculated for establishment of the traceability and reference metrology of the line width measurement by estimating the other contributors and the thickness of oxide film.

REFERENCES

1. Nakayama, Y., Gonda, S., Misumi, I., Kurosawa, T., Kitta, J. Mine, H., Sasada, K., Yoneda, S. and Mizuno, T., "Novel CD-SEM calibration reference patterned by EB cell projection lithography," Proc. SPIE 5752, 591-602 (2005).
2. Yamaguchi, A., Fukuda, H., Kawada, H. and Iizumi, T., "Impact of long-edge roughness (LER) on accuracy in critical dimension measurement and new guideline for CD metrology," Jpn. J. Appl. Phys. 44, 5575-5580 (2005).
3. Villarrubia, J. S., Vladar, A. E. and Postek, M. T., "A simulation study of repeatability and bias in the CD-SEM," Proc. SPIE 5038, 138-149 (2003).
4. Nakayama, Y., Kawada, H., Yoneda, S. and Mizuno, T., "Novel CD-SEM calibration reference consisting of 100-nm pitch grating and positional identification mark," Proc. SPIE 6518, 65183J (2007).
5. Abe, H., Hamaguchi, A. and Yamazaki, Y., "Evaluation of CD-SEM measurement uncertainty using secondary electron simulation with charging effect," Proc. SPIE 6518, 65180L (2007).
6. Dixson, R. and Orji, N. G., "Comparison and uncertainties of standards for critical dimension atomic force microscope tip width calibration," Proc. SPIE 6518, 651816 (2007).
7. Hasler-Grohne, W., Frase, C. G., Czerkas, S., Dirscherl, K., Bodermann, B., Mirande, W., Ehret, G., and Bosse, H., "Calibration procedures and application of the PTB photomask CD standard," Proc. SPIE 5992, 59924O (2005).
8. Bosse, H., Mirande, W. and Frase, C. G., "Comparison of linewidth measurements on COG masks," Proc. SPIE 4349, 99-108 (2001).
9. Lowney, J. R., "Use of Monte Carlo modeling for interpreting scanning electron microscope linewidth measurements," Scanning 17, 281-286 (1995).
10. Liu, H.-C., Fong, D., Dahlen, G. A., Osborn, M., Hand, S. and Osborne, J. R., "Carbon nanotube AFM probes form microlithography process control," Proc. SPIE 6152, 61522Y (2006).
11. http://www.hitachi-hitec.com/global/em/fib/fib_index.html
12. http://www.hitachi-hitec.com/global/em/tem/tem_index.html
13. http://physics.nist.gov/cgi-bin/cuu/Value?asil
14. Barth, J. V., Costantini, G. and Kern, K., "Engineering atomic and molecular nanostructures at surfaces," Nature 437, 671-679 (2005).
15. Larkin, K. G., Oldfieldb, M. A. and Klemma, H., "Fast Fourier method for the accurate rotation of sampled images", Optics Communications 139, 99-106 (1997).
16. Brigham, E. O., "The fast Fourier transform and its applications," Prentice-Hall, Englewood Cliffs, NJ, (1988).